

SWIFT/UVOT GRISM MONITORING OF NGC 5548 IN 2013: AN ATTEMPT AT MG II REVERBERATION MAPPING

E. M. CACKETT¹, K. GÜLTEKIN², M. C. BENTZ³, M. M. FAUSNAUGH⁴, B. M. PETERSON^{4,5}, J. TROYER¹, AND M. VESTERGAARD^{6,7}

¹Department of Physics & Astronomy, Wayne State University, 666 W. Hancock St, Detroit, MI 48201, USA

²Department of Astronomy, University of Michigan, 1085 S. University Ave, Ann Arbor, MI 48109, USA

³Department of Physics & Astronomy, Georgia State University, Atlanta, GA 30303, USA

⁴Department of Astronomy, The Ohio State University, 140 West 18th Ave, Columbus, OH 43210, USA

⁵Center for Cosmology and Astroparticle Physics, The Ohio State University, 191 West Woodruff Ave, Columbus, OH 43210, USA

⁶Dark Cosmology Centre, The Niels Bohr Institute, Juliane Maries Vej 30, DK-2100 Copenhagen Ø, Denmark and

⁷Steward Observatory, University of Arizona, 933 N Cherry Avenue, Tucson, AZ 85721, USA

Draft version September 27, 2018

ABSTRACT

Reverberation-mapping-based scaling relations are often used to estimate the masses of black holes from single-epoch spectra of AGN. While the radius–luminosity relation that is the basis of these scaling relations is determined using reverberation mapping of the $H\beta$ line in nearby AGN, the scaling relations are often extended to use other broad emission lines, such as Mg II, in order to get black hole masses at higher redshifts when $H\beta$ is redshifted out of the optical waveband. However, there is no radius-luminosity relation determined directly from Mg II. Here, we present an attempt to perform reverberation mapping using Mg II in the well-studied nearby Seyfert 1, NGC 5548. We used *Swift* to obtain UV grism spectra of NGC 5548 once every two days from April to September 2013. Concurrent photometric UV monitoring with *Swift* provides a well determined continuum lightcurve that shows strong variability. The Mg II emission line, however, is not strongly correlated with the continuum variability, and there is no significant lag between the two. We discuss these results in the context of using Mg II scaling relations to estimate high-redshift black hole masses.

Subject headings: galaxies: active — galaxies: individual (NGC 5548) — galaxies: nuclei — galaxies: Seyfert

1. INTRODUCTION

The mass of supermassive black holes (SMBHs) at the centers of galaxies, and their evolution with time is an important part of the picture of galaxy formation and evolution, as strong correlations between galaxy and black hole properties suggest they are closely connected, e.g., through the M – σ and M – L relations (e.g., Gebhardt et al. 2000; Magorrian et al. 1998; Gültekin et al. 2009; Kormendy & Ho 2013). Much effort over the last several decades has gone into determining the masses of SMBHs in nearby galaxies, through methods such as those using stellar (e.g., Gültekin et al. 2014) and gas dynamics (e.g., Walsh et al. 2013), or reverberation mapping (e.g., Peterson et al. 2004; Bentz et al. 2009b). This nearby sample of SMBHs with black hole mass measurements can then form the basis of scaling relations that can be applied to much more distant objects where direct methods are not possible. One of the most powerful of these scaling relations is the radius-luminosity, R – L , relation which relates the size of the broad emission line region (BLR) in an active galactic nucleus (AGN), as measured by reverberation mapping, to the AGN luminosity.

The basic principle behind reverberation mapping is simple. In AGNs, large amounts of photoionized gas moves under the influence of the central SMBH’s gravity, allowing a direct measurement of the velocity dispersion in the BLR. To determine a mass, the radius of the BLR from the SMBH is needed, which can be obtained using the reverberation mapping technique (Blandford & McKee 1982; Peterson 1993, 2014). In this method, the observed time lag, τ , between an emission line lightcurve (typically $H\beta$) and the optical continuum lightcurve is interpreted as the light-travel time from the continuum emitting region close to the SMBH and the

BLR further out (where the continuum is reprocessed into line emission). The lag thus gives the emissivity-weighted average radius of the BLR, $R = \tau c$. Combining some measure of the width of the emission line used and the radius leads to a mass measurement via the virial theorem. In this way, reverberation mapping has successfully determined the masses of ~ 60 supermassive BHs in AGNs (e.g., Peterson et al. 2004; Bentz et al. 2009b; Barth et al. 2011; Pancoast et al. 2014; Barth et al. 2015; Bentz & Katz 2015).

Such mass measurements have allowed the determination of the R – L scaling relation (Kaspi et al. 2000; Bentz et al. 2006b, 2009a, 2013), which is based on the time lag (and hence radius) obtained using the $H\beta$ broad emission line. The R – L relation leads to a mass estimate from a single-epoch AGN spectrum — a measurement of the AGN luminosity gives the BLR radius from the R – L relation, and the broad emission line width can be used to determine the line of sight velocity dispersion. This therefore allows estimates of black hole masses in large samples of galaxies (e.g. Vestergaard 2002; McLure & Jarvis 2002; Vestergaard & Peterson 2006; Vestergaard & Osmer 2009). The R – L relation has also successfully been used to discover low-mass ($M_{\text{BH}} < 2 \times 10^6 M_{\odot}$) AGN (Greene & Ho 2007; Baldassare et al. 2015).

The R – L relationship is well-established for $H\beta$, which is easily observed with ground-based observations in the case of local AGNs. However, as z increases, $H\beta$ is shifted to IR wavelengths that become less accessible. At higher redshifts, it is thus desirable to use instead strong rest-frame UV lines, such as C IV $\lambda 1549$ and Mg II $\lambda 2798$. Unfortunately, the R – L relationship is poorly established for C IV and is heavily dependent on one provisional measurement of a high-luminosity quasar (Kaspi et al. 2007). However, gravitational microlensing has allowed measurements of the size of the high-ionization BLR in gravitationally lensed systems,

and these data support an $R-L$ relationship that is parallel to that of $H\beta$ (Guerras et al. 2013). The situation is even worse for Mg II as there are only two reliable Mg II lags that have been measured, NGC 3783 (Reichert et al. 1994) and NGC 4151, for which there are two independent measurements (Metzroth et al. 2006). Thus far, the best that can be done in the absence of suitable C IV and Mg II reverberation measurements is to assume these lines have $R-L$ relationships that are parallel to that for $H\beta$ and assume that all lines yield the same black hole mass, so that the quantity $VP = R\Delta V^2/G$, where ΔV is the line width, is constant (Onken & Kollmeier 2008; McGill et al. 2008; Rafiee & Hall 2011; Shen & Liu 2012; Park et al. 2013). Note that in all cases where it has been testable, VP is found to be consistent between different emission lines (Peterson & Wandel 1999, 2000; Kollatschny 2003; Peterson et al. 2004; Bentz et al. 2010).

Calibration of the black hole mass scale requires another step, usually written as $M_{\text{BH}} = fVP$, where f is a dimensionless factor of order unity that depends on the BLR orientation and other generally poorly known parameters. The factor f is thus expected to vary from system to system, but the consistency of the virial product for multiple lines in a given system suggests that f is also approximately constant for a given system. With the most recent direct modeling of high-quality reverberation data, it is possible to uniquely model f for a given system (Brewer et al. 2011; Pancoast et al. 2014), but at this time only a few such measurements have been made. What is usually done instead is to compute an ensemble average value for $\langle f \rangle$ by using another estimate of the black hole mass, in practice from the $M-\sigma$ relationship. Two recent estimates from this method give $\langle f \rangle = 4.31 \pm 1.05$ (Grier et al. 2013) and $\langle f \rangle = 4.47 \pm 1.24$ (Woo et al. 2015). Interestingly, these are consistent with the average of the 5 individual f values determined from direct modeling by Pancoast et al. (2014) (see that paper for a detailed discussion comparing f values from the two independent and separate approaches).

There has been debate about the reliability of using C IV and Mg II for black hole mass estimates. For instance, Mg II is systematically narrower than $H\beta$ (Wang et al. 2009; Marziani et al. 2013), but may be more reliable than C IV (Trakhtenbrot & Netzer 2012). However, other studies have shown no net bias in using these rest-frame UV lines (Greene et al. 2010; Rafiee & Hall 2011), and good agreement with $H\beta$ -based masses (Assef et al. 2011). Furthermore, the discrepancies and scatter in the relations can be a result of the non-variable component of line profile (Denney 2012) and low signal-to-noise ratio spectra that do not allow for an accurate characterization of the line profile (Denney et al. 2013). Even so, measuring reverberation of Mg II remains an important goal in order to further validate these scaling routines. Thus far, there has only been one Mg II mass determined (NGC 4151, Metzroth et al. 2006) using archival *IUE* data, which gives a value consistent with the $H\beta$ mass (Bentz et al. 2006a).

As discussed above, there have only been two objects where a Mg II lag has been successfully recovered (Reichert et al. 1994; Metzroth et al. 2006). It is useful to discuss other cases where reverberation of Mg II has been looked for, and where the variability of Mg II has been studied. One of the more intense monitoring campaigns that looked for Mg II variability was the 1989 *IUE* campaign of NGC 5548 (Clavel et al. 1991). While there was significant variability in the continuum (ratio of maximum to minimum flux ~ 4.5) and high-

ionization lines, Mg II was the least variable with a maximum to minimum flux ratio of ~ 1.3 . Clavel et al. (1991) attempted to measure a lag but found it was not well constrained, with $\tau = 34-72$ days. During the monitoring campaign of NGC 3783, even though Reichert et al. (1994) were successfully able to measure a lag, Mg II is again the least variable emission line, and the authors worry about whether variable Fe II contributes to the Mg II variability. No other studies have had the intense monitoring required to attempt Mg II reverberation, however, there are a number of studies looking at Mg II variability from fewer observations. Five *HST* observations of NGC 3516 also showed significant lack of variability in Mg II, with the variability constrained to be less than 7% even though the UV continuum varied by a factor of 5 (Goad et al. 1999b,a). More recent observations of Mg II variability in higher luminosity quasars have found mixed results. For instance, Woo (2008) found significant variability (8–17% rms) in 4 of the 5 quasars studied over 1–1.5 year rest-frame timescales, and Hryniewicz et al. (2014) find a 25% change in Mg II flux in the quasar LBQS 211–4538 from observations 6 months apart. On the other hand, little or no Mg II variability is seen in studies of two other quasars (Trevese et al. 2007; Modzelewska et al. 2014). Finally, a study of spectral variability of quasars in the SDSS Stripe 82 region found Mg II variability to be weak, and less variable compared to Balmer emission lines (Kokubo et al. 2014). Thus, there are a number of examples of low variability in Mg II, with only a few exceptions, and very few attempts at Mg II reverberation mapping.

The *Swift*/UVOT allows a route to doing UV reverberation mapping using the U grism onboard. *Swift*'s observing schedule is flexible, allowing for short (1 or 2 ks) daily monitoring of AGN. The effective area of the U grism peaks at around the wavelength of Mg II, and thus can, in principle, be used to perform direct Mg II reverberation mapping. In order to expand the number of AGN with Mg II reverberation mapping, and as a first step towards an ultimate goal of determining a Mg II $R-L$ relation, we undertook a long-term (~ 6 month) monitoring campaign of NGC 5548 in 2013. NGC 5548 (an S0/a Seyfert galaxy at $z = 0.01718$) was chosen since it is the best-studied reverberation-mapped AGN to date, with many years of monitoring (see, e.g., Peterson et al. 2002; Bentz et al. 2007, 2010; De Rosa et al. 2015; Edelson et al. 2015, and references therein), and also had previous *IUE* data (Clavel et al. 1991) to allow for a feasibility study.

Our *Swift*/UVOT U grism monitoring campaign of NGC 5548 took place from 2013 April 1 to September 12 (PI: Cackett). We have also supplemented the UV continuum lightcurve with concurrent *Swift* photometric monitoring that took place immediately before and during our grism campaign. An analysis of the UV photometric lightcurves during this period has already been presented by both Kaastra et al. (2014) and McHardy et al. (2014). Furthermore, the broadband spectral energy distribution of NGC 5548 during this period (including *Swift* U grism spectra) has been examined by Mehdipour et al. (2015).

The data reduction is described in Section 2, and our time series analysis is given in Section 3. We discuss our results and their implications in Section 4.

2. DATA REDUCTION

2.1. UV grism data

Grism observations were taken from 2013 April 1 to 2013 September 12 approximately once every two days (on average). Each observation typically consists of a total of 2 ksec exposure time on the source. However, this is usually performed as two separate ~ 1 ksec exposures, taken within a couple of hours of each other. The *Swift* target IDs of the grism observations are 91711, 91737 and 91739. Of the total 82 grism observations, 7 (all target ID 91737) were taken at a roll angle where a nearby star was dispersed adjacent to the dispersed NGC 5548 spectrum. It was not possible to cleanly extract a spectrum from these observations that did not contain continuum emission from the star. Excluding those 7 observations, we are left with a total of 75 grism observations of NGC 5548. Of the remaining 75 observations, 7 exposures (target ID 91739) had a roll angle that put a zeroth-order image of a star at approximately 2000 \AA in the dispersed first order spectrum of NGC 5548. These observations could not be used for the mean and rms spectrum, but we were still able to calculate line fluxes because the first order spectrum around the Mg II line is not contaminated.

To perform the *Swift*/UVOT grism data analysis, we use Paul Kuin’s UVOTPY software version 2.0.3 (Kuin 2014), which is designed specifically for analysis of *Swift*/UVOT grism data. Details of the calibration of the *Swift*/UVOT grism and of the software are given in Kuin et al. (2015).

We extract the grism spectrum using the `uvotgetspec` tool, and default parameters for the width of the extraction regions for the source and background. For the vast majority of observations, a short UVW2 image is taken during the same pointing. Since with grism spectroscopy the wavelength scale depends on the location of the zeroth-order image, the software uses the UVW2 image in order to anchor the wavelength scale. In a small number of pointings, no photometric image was taken, leading to a more poorly defined anchor position.

The 1σ wavelength accuracy of the UV grism in clocked mode is 9 \AA (Kuin et al. 2015), thus, we use the Mg II line itself in order to provide a better wavelength determination. For each spectrum we find the centroid of the Mg II using the wavelength range where the flux of the line is $\geq 70\%$ of the peak value. We find a mean absolute wavelength shift of 9 \AA when a photometric image has been taken (consistent with the *Swift* calibration: Kuin et al. 2015), and 39 \AA when no photometric image exists.

Once the wavelength shifts have been applied, we calculate the mean and root mean square (rms) spectra, shown in Figure 1. All flux densities are given in the emitted frame, and are corrected for Galactic reddening assuming $E(B-V) = 0.0199$ (Schlegel et al. 1998) and the dust reddening law of Seaton (1979). We use Seaton (1979) for easy comparison with previous work on NGC 5548 which also use this reddening law, though the choice does not make any difference in determining lags. The effective area of the UV grism drops off rapidly at about 1800 \AA . Furthermore, at wavelengths longer than about 3000 \AA the second-order spectrum can overlap and contaminate the first-order spectrum. We therefore concentrate on the spectrum between $1800\text{--}3400 \text{ \AA}$. The Mg II line at a rest wavelength of 2798 \AA can clearly be seen. Other features in the spectrum include the C III] $\lambda 1909$ semi-forbidden emission line, and the Fe II emission line complex (most prominent in the region $2200\text{--}2800 \text{ \AA}$, see e.g. Baldwin et al. 2004). Mehdipour et al. (2015) present a fit to the broadband spectral energy distribution of NGC 5548, which includes the mean

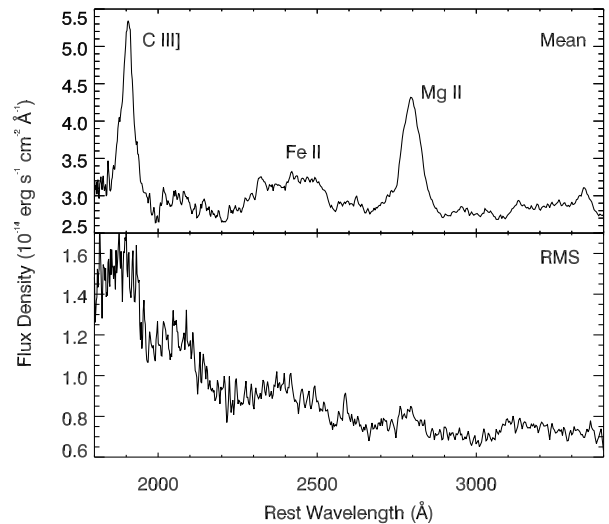


FIG. 1.— *Top*: Mean UV grism spectrum of NGC 5548. The C III] and Mg II emission lines are clearly visible. The Fe II emission line complex extends either side of the Mg II line but is most prominent from $2200\text{--}2800 \text{ \AA}$. *Bottom*: Root mean square UV grism spectrum of NGC 5548.

UV grism spectrum, and the reader is referred to that paper for more details on individual components. In the rms spectrum, the Mg II can be identified, but it is not a strong feature, already indicating that it is not highly variable during our monitoring of NGC 5548. The mean continuum flux at 2670 \AA is approximately the same as during the 1989 *IUE* observations presented by Clavel et al. (1991).

The Mg II line is well modeled by a single Gaussian. Both a direct measurement and the best-fitting Gaussian give a $\text{FWHM} = 68 \text{ \AA}$. However, this does not take into account the significant instrumental broadening. Unfortunately, the line spread function is not accurately known at all wavelengths (N. P. M. Kuin, private communication). The resolving power is given as $R = 75$ at 2600 \AA (Kuin et al. 2015), which for the observed wavelength of Mg II corresponds to $\Delta\lambda = 38 \text{ \AA}$. Correcting for this broadening (assuming a Gaussian with $\text{FWHM} = 38 \text{ \AA}$) gives an intrinsic $\text{FWHM} = 56.5 \text{ \AA}$, or $\Delta v = 5960 \text{ km s}^{-1}$. For comparison, the FWHM of $H\beta$ in NGC 5548 has been seen to range from 3078 km s^{-1} (Peterson et al. 2002) to 11177 km s^{-1} (Bentz et al. 2010), with line width anti-correlated with AGN luminosity.

2.2. Photometric data

As described above, NGC 5548 was monitored intensely with *Swift* during 2013. UVW2 was the filter most commonly used throughout the monitoring, thus, we use those data to determine the UV continuum lightcurve covering the period immediately before and throughout our grism monitoring. In addition to the UVW2 observations associated with our grism observations (117 observations in total), we take advantage of other, shorter, photometric monitoring campaigns of NGC 5548 taking place at the same time: target IDs 91404 (32 observations between 2012 November 17 and 2013 March 29, PI: McHardy), 91744 (50 observations, PI: Kaastra) and 30022 (17 observations). Before 2013 April 1, photometric monitoring was approximately once every 4 days. Beginning 2013 April 1 when our grism monitoring began, the cadence increased to once every 2 days, and from the end of May until mid-September monitoring occurred more frequently, some-

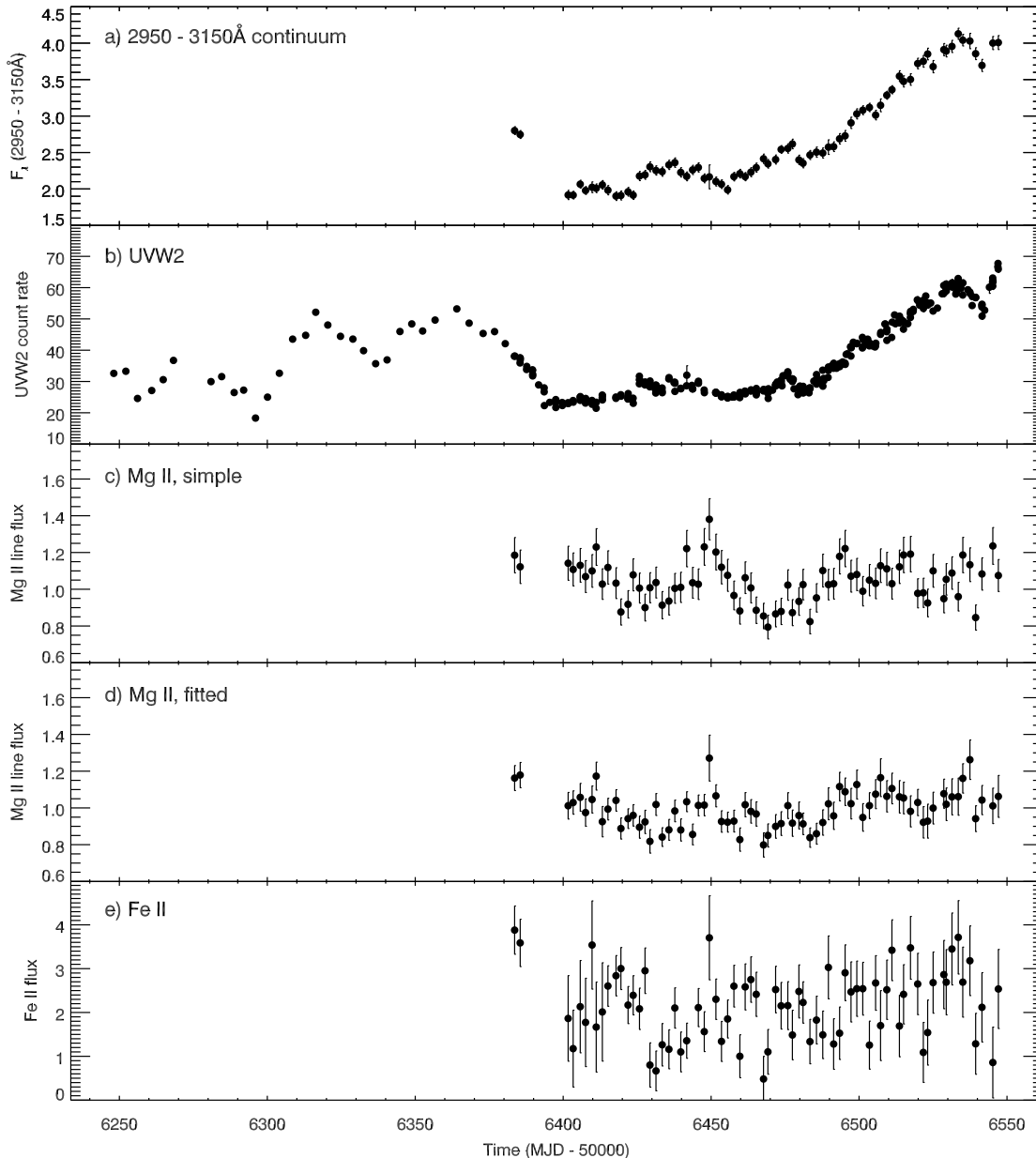


FIG. 2.— *a)* Average flux density between 2950 and 3150 Å in units of 10^{-13} erg s^{-1} cm^{-2} \AA^{-1} . *b)* *Swift*/UVW2 count rate in counts per second. *c)* Integrated Mg II line flux in units of 10^{-12} erg s^{-1} cm^{-2} from the simple approach to determining the Mg II line flux. *d)* Integrated Mg II line flux in units of 10^{-12} erg s^{-1} cm^{-2} from the Fe template fitting approach to determining the Mg II line flux. *e)* Fe II flux integrated over the 2000 – 3000 Å region in units of 10^{-12} erg s^{-1} cm^{-2} determined from Fe template fitting.

times with two observations per day. In total we analyzed 216 observations between 2012 November 17 and 2013 September 12.

The UVW2 observations are often split into two separate pointings. Rather than combine all pointings within a given day together, we analyze them separately in order to get the highest time cadence. The UVW2 photometric lightcurve (along with other filters) during this period has already been presented by Kaastra et al. (2014), McHardy et al. (2014), Mehdipour et al. (2015) and Edelson et al. (2015). We perform photometry on NGC 5548 using `uvotsource` with a $5''$ circular source extraction region, and a $10''$ background region offset from the galaxy. As described by McHardy et al. (2014), Mehdipour et al. (2015) and Edelson et al. (2015) a

small number of observations were found to be anomalously low ($>15\%$ lower) compared to the surrounding local mean, with the origin thought to be instrumental rather than intrinsic to the source. We manually removed these “drop-outs” from the lightcurve (see McHardy et al. 2014, Mehdipour et al. 2015 and Edelson et al. 2015 for more detailed discussion). The UVW2 photometric lightcurve is shown in panel b) of Figure 2.

2.3. UV continuum and Mg II lightcurves

We use the individual grism spectra to determine the UV continuum flux and Mg II lightcurves. For the UV continuum lightcurve, we calculate the mean flux density from 2950 to 3150 Å. This lightcurve is also shown in panel a) of Figure 2.

As can be seen, the 2950–3150 Å lightcurve is strongly correlated with the UVW2 lightcurve. The UVW2 bandpass peaks at a shorter wavelength at about 2100 Å and the effective area drops off significantly by 3000 Å. Figure 3 shows the UVW2 count rate versus the 2950–3150 Å continuum flux, demonstrating the strong correlation between the two. The UVW2 is highly variable with a variability amplitude (Vaughan et al. 2003) of $F_{\text{var}} = 0.33$.

To determine the Mg II line flux we take two approaches. First we take a simple approach involving defining the continuum in regions either side of the line, as is typically done in AGN reverberation studies, since the goal is to capture the line flux *variations* in a model-independent fashion, rather than to capture all the line flux. Second, we perform multi-component spectral fitting to try and separate the contribution of the Fe II complex from the Mg II line and continuum.

2.3.1. Mg II line flux: simple approach

In this first approach, we determine the Mg II integrated line flux by fitting the local continuum either side of the line. We fit a straight line to the continuum including data in the ranges 2560–2695 Å and 2950–3150 Å. We then integrate the line flux above the continuum from 2695–2900 Å. The line lightcurve from this method is also shown in panel c) of Figure 2. We find that the uncertainties in line flux estimated directly from the uncertainties in individual flux bins appears to be overestimated, with mean fractional uncertainty in the line flux being 0.134. We verified this overestimate by comparing flux differences between data points on timescales as short as 2 days. Assuming those flux differences are stochastic, and that the fractional error is the same on all points, we get a fractional error of 0.081. This is an upper limit on the flux uncertainties since there may be intrinsic flux variability on two-day timescales. We adopt fractional errors of 0.081 on the Mg II line flux measurements. The lightcurve only has small amplitude variability, with $F_{\text{var}} = 0.074$. By eye, there does not appear to be a correlation between the continuum and Mg II lightcurves, and this is also clear when looking at UVW2 count rate versus Mg II line flux in Figure 3.

We also explore the continuum lightcurves at different wavelengths, calculating the mean flux density between 2015–2215 Å and also 4430–4625 Å. We compare these lightcurves in Figure 4. The lightcurves are clearly correlated, and there is an obvious decrease in variability amplitude with increasing wavelength. This decrease in variability amplitude with wavelength can also be seen in the rms spectrum (Fig. 1). The lightcurves indicate that the spectrum is bluer when brighter.

2.3.2. Fe template fitting

Strong Fe II emission is visible in the spectrum, and thus to determine more robustly the Mg II line flux we perform multi-component spectral fitting in order to decompose the Fe II, Mg II and continuum components. A similar Fe template fitting approach has been used by Barth et al. (2013) to successfully recover optical Fe II lags in two AGN.

For the Fe II line complex we use the template model of Vestergaard & Wilkes (2001). In addition to the Fe template, we also include a power-law continuum and a Gaussian to model the Mg II line. The model is then convolved with a Gaussian with FWHM = 38 Å to match the instrument resolution and fitted to the individual spectra in the 2000 – 3000 Å region.

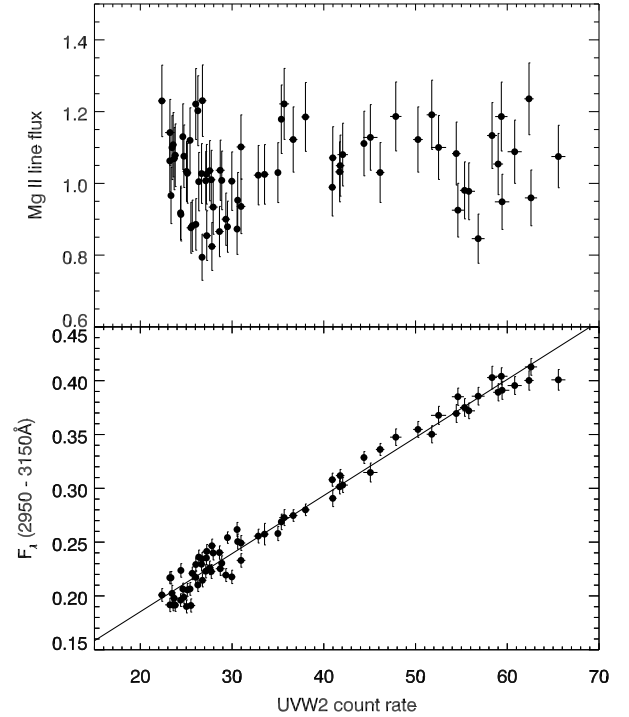


FIG. 3.— *Top*: Mg II line flux (10^{-12} erg s^{-1} cm^{-2}) from the simple method versus UVW2 count rate (c/s). No correlation is apparent. *Bottom*: 2950–3150 Å flux density (10^{-13} erg s^{-1} cm^{-2} Å $^{-1}$) versus UVW2 count rate. There is a clear, strong correlation, with the best-fitting straight line shown.

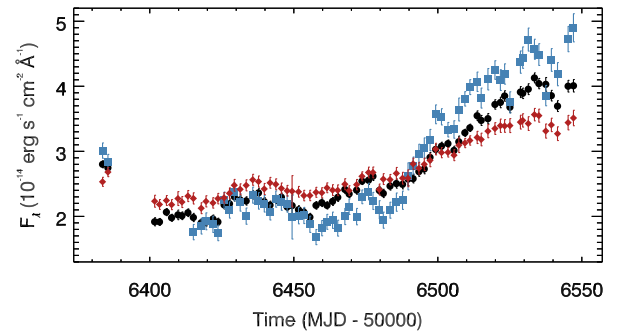


FIG. 4.— Continuum lightcurves from the U grism in 2015–2215 Å (blue squares), 2950–3150 Å (black circles), and 4430–4625 Å (red diamonds). They are all clearly correlated, but there is no significantly detected lag. The amplitude of variability decreases with increasing wavelength, as expected for disk reverberation.

When fitting this model, we consistently found reduced- χ^2 values significantly less than 1.0, once again indicating that the uncertainties in the flux from `uvotsource` appear to be overestimated. We therefore scale the uncertainties by $\sqrt{\chi^2_{\nu}}$: the mean scale factor is 0.5.

Figure 5 shows a spectral fit, using the first *Swift* observation in April 2013 (obsID: 00091711002) as an example. The example demonstrates how the Fe II emission overlaps with the Mg II line.

There is good agreement between the line flux determined by the simple approach and the Fe template fitting method. We show the Mg II lightcurve from this method in panel d) of Figure 2, and a comparison of the line fluxes from both methods in Figure 6. The Mg II flux is slightly lower when deter-

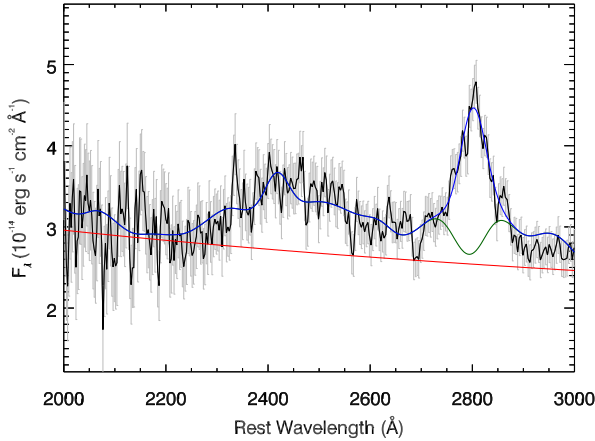


FIG. 5.— *Swift* U grism spectrum of NGC 5548 from observation 00091711002. The blue line shows the best-fitting spectral model, consisting of the power-law continuum (red), Fe template and a Gaussian to model the Mg II line. The green line shows the model minus the Mg II line.

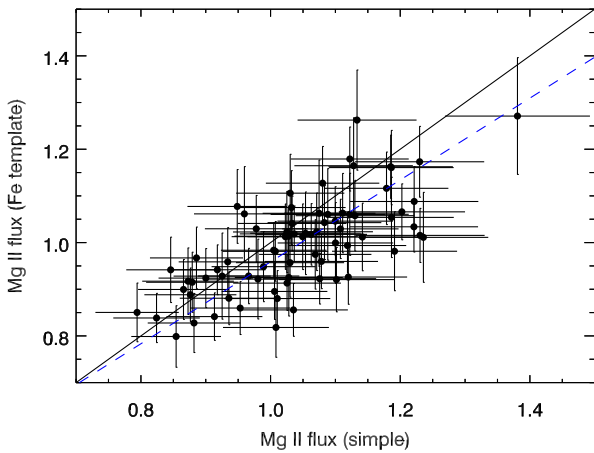


FIG. 6.— A comparison of the Mg II line flux (10^{-12} erg s^{-1} cm^{-2}) determined from the simple method and the Fe template fitting method. The black solid line shows $x = y$, while the dashed blue line shows the best-fitting straight line.

mined from the Fe template fitting method, because a small amount of Fe contributes to the total flux within the wavelength limits of the Mg II emission line. The mean fractional uncertainty in the Mg II line flux is 0.073 from this method, very similar to what we estimated for the simple method based on variability between adjacent data points.

The integrated flux from the Fe II line complex over the 2000 – 3000 Å region is shown in panel e) of Figure 2. However, the Fe II flux is poorly constrained from the spectral fitting, with a mean fractional uncertainty of 0.29. The resulting lightcurve is noisy with no clear variability pattern. Since the individual spectra are reasonably noisy, and the response of Fe II is expected to be longer than that of H β (Vestergaard & Peterson 2005), we also tried binning the spectra in time, by up to 5 epochs, to improve the lightcurve. While this reduces scatter in the lightcurve, it does not show any clear correlated variability with the continuum lightcurve.

3. CROSS CORRELATION ANALYSIS

We use the standard cross correlation analysis techniques to determine if there is a time lag between the UV continuum and the Mg II line. Since the UVW2 lightcurve is sig-

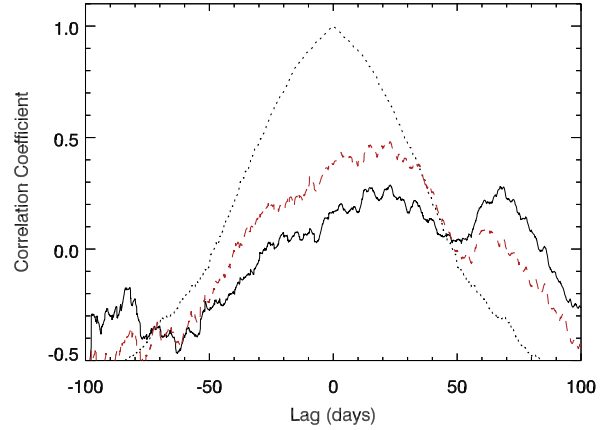


FIG. 7.— The solid line shows the cross-correlation function (CCF) between the UVW2 and Mg II lightcurves when using the simple flux calculation method, the red dashed line shows the CCF when using the Mg II lightcurve determined through Fe template fitting. The low peak value of the CCF indicates no significant correlation or lag. The dotted line shows the auto-correlation function of the UVW2 lightcurve.

nificantly longer than the 2950–3150 Å lightcurve, we use the UVW2 lightcurve to search for a lag. We calculate the cross correlation function (CCF) between the Mg II and UVW2 lightcurves, using the linear interpolation method as described by White & Peterson (1994). The CCFs are shown in Figure 7 when using the Mg II lightcurves determined both from the simple and Fe template fitting methods. Regardless of the Mg II lightcurve used there are two peaks in the CCF with one at approximately 20 days and the other at approximately 70 days. However, the CCF does not peak at a high value (the peak is < 0.5 for both Mg II lightcurves), indicating that the UVW2 and Mg II lightcurves are not strongly correlated.

We use the standard Monte Carlo flux randomization/random subset sampling method as implemented by Peterson et al. (2004) in order to generate 10,000 pairs of lightcurves, and we determine the peak and centroid value of the CCF for each pair. We use the mean value of the distribution centroid values as our best value for lag centroid, τ_{cent} , though we note that the centroid distribution is also double peaked, like the CCF. We find $\tau_{\text{cent}} = 34^{+34}_{-24}$ days when using the Mg II lightcurve from the simple method and $\tau_{\text{cent}} = 13^{+11}_{-12}$ days when using the Fe template method lightcurve, again indicating there is no significant non-zero lag. Note that the CCFs from both methods peak at around 20 days, and the difference in centroid lags comes from the stronger secondary peak at 70 days in the CCF from the simple method. We also note that the peak in the CCF that can be seen at around 70 days in Figure 7 is narrower than the auto-correlation function (ACF) of the UVW2 lightcurve, and thus likely not real. If the line lightcurve is formed in response to changes in the continuum lightcurve then the CCF will be the ACF convolved with the transfer function, and so should be broader (not narrower) than the ACF. Furthermore, the ACF of the Mg II lightcurve is very narrow, with a secondary peak at 50 days. As noted when discussing the Fe II lightcurve, we also tried binning up the spectra in time by up to 5 epochs, however, this also led to no lag detection in Mg II.

We also determine whether there is any significant lag between the UVW2 and grism continuum lightcurves. Since the grism lightcurves are close to monotonic, we take out the long term trends in the lightcurves by fitting a low-order polynomial, and subtracting it from the data. Such detrending is

shown to improve lag measurements (Welsh 1999), and since we expect the interband lags to be short removing the long-term trends reduces aliasing effects. The lags measured relative to the UVW2 are $\tau_{\text{cent}} = -0.9_{-0.9}^{+0.8}$ days, $\tau_{\text{cent}} = 1.1_{-0.5}^{+0.7}$ days and $\tau_{\text{cent}} = 0.3_{-1.9}^{+0.9}$ days, for the 2015–2215 Å, 2950–3150 Å, and 4430–4625 Å lightcurves respectively.

Wavelength-dependent continuum lags are expected from disk reverberation (thermal reprocessing), where the inner, hotter accretion disk responds to variations in the irradiating flux before the outer, cooler disk (see Cackett et al. 2007, for a detailed description). McHardy et al. (2014) use the photometric lightcurves during the 2013 campaign to provide a measure of these wavelength-dependent lags, and the even higher cadence *Swift* monitoring in 2014 have provided an extremely good measure of these (Edelson et al. 2015). While none of our interband lags are significantly non-zero, they are consistent with those expected based on Edelson et al. (2015).

4. DISCUSSION

We monitored NGC 5548 for approximately 170 days with the U grism onboard *Swift* during 2013, obtaining low-resolution UV spectra approximately every other day during the monitoring campaign. By combining these spectra with photometric monitoring before and during our grism campaign, we attempted to compare the variability of the continuum and Mg II emission line. The UV continuum showed significant variability over the campaign, though the flux changes were almost a monotonic increase over the period of grism monitoring. The Mg II emission line, however, was not significantly variable, and hence there is no plausible lag between the continuum and emission line, preventing a reverberation mapping mass estimate from the Mg II line alone.

Even though not significant, it is interesting to note that the peak in the CCF between the UV continuum and Mg II line at approximately 70 days is consistent with the largest peak in the equivalent CCF for Mg II from the *IUE* monitoring campaign of 1989 (Clavel et al. 1991), though that peak is also of low significance, and quite probably a result of aliasing. An important consideration is whether the lack of response to continuum variability is due to an intrinsic property of the line, the location of the Mg II line emitting region, or whether the near monotonic increase in continuum flux over the grism monitoring period prevented a clear lag measurement. Mg II is a low excitation line, thus is emitted from a region further away from the central AGN than other BLR lines such as H β or C IV. This location further from the AGN could be why we do not see a clear response to continuum variability. If the inner part of the BLR blocks a clean view of the central engine, the Mg II emitting region may see only scattered continuum emission. Certainly there is significant absorbing and obscuring material in the inner region of NGC 5548 as evidenced by the large number of absorption lines seen during both 2013 and 2014 *HST* observations of NGC 5548 (Kaastra et al. 2014; De Rosa et al. 2015). How absorption affects the Mg II line which is actually a resonant doublet, and how changes in the absorption affect the line variability are not clear since the grism data are not high enough resolution to detect any narrow absorption lines. Such issues are known to cause problems in accurately determining the line profile (Denney et al. 2013). On the other hand, the fact that the continuum lightcurve during the grism observations shows a near-monotonic increase with no strong peaks or troughs, means that it would be hard to see a clear response from the line. The photometric moni-

toring that took place immediately before our grism observations began does show several strong variable features, however the lag would have to be almost 100 days to see the two clear peaks in that lightcurve.

It is also important to consider the photoionization properties of Mg II. The observed response of a line to continuum fluctuations will depend both on its local responsivity, that is the marginal response of the line to continuum variations, and geometric dilution, i.e. the blurring of the response due to the distribution of delays set by the geometry of the BLR. Photoionization calculations show the responsivity for Mg II to be low compared to high ionization lines (Goad et al. 1993; O’Brien et al. 1995; Korista & Goad 2000), meaning that the line should not be expected to respond strongly to changes in continuum flux. For instance, figure 7 of Goad et al. (1993) which shows how the responsivity for Mg II compares to other lines. This can also be seen in figure 2b of Korista & Goad (2000), which shows that the EW of Mg II is generally strongly negatively correlated with the incident ionizing photon flux. This equates to generally small values in the local gas responsivity for Mg II, and also results in large centroids in delay in its 1D transfer function. The latter makes this line’s response also susceptible to geometric dilution. The result is a small response amplitude in Mg II, compared to the other UV emission lines (see also figure 5a of Korista & Goad 2000). Thus, the lack of variability of Mg II could be due to an intrinsic property of the line, as suggested by Goad et al. (1999a) when discussing the lack of Mg II variability in NGC 3516.

It would be valuable to be able to measure Mg II reverberation mapping masses directly (as we discussed in section 1). Unfortunately, the lack of significant lag prevents us from doing this. Although a direct reverberation mapping mass was not possible, we can still use the mean spectrum in order to obtain a ‘single-epoch’ Mg II mass estimate to compare with the well-constrained H β mass for NGC 5548. To get a ‘single-epoch’ mass measurement, we combine the line width ($\sigma = 2351 \text{ km s}^{-1}$) with the mean continuum luminosity at 3000 Å, $\lambda L_{\lambda}(3000 \text{ Å}) = 5.2 \times 10^{43} \text{ erg s}^{-1}$, and use the relation of McGill et al. (2008) to estimate $M_{\text{BH}} = 7 \times 10^7 M_{\odot}$. This is slightly larger than, though still in reasonable agreement with, the H β reverberation mapping mass for NGC 5548 of $5.95 \times 10^7 M_{\odot}$ (assuming an f -factor; Grier et al. 2013), and $3.2 \times 10^7 M_{\odot}$ (from direct modeling; Pancoast et al. 2014).

In summary, we do not detect a significant lag between the Mg II and UV continuum flux in NGC 5548 from a ~ 6 month monitoring campaign with *Swift*. However, *Swift*’s ability to perform long-term monitoring of nearby Seyfert 1s and obtain crude UV spectra could lead to the measurement of a Mg II lag in other bright AGN if the Mg II line is variable enough.

We thank the *Swift* team for their hard work and efforts in successfully scheduled this monitoring campaign. Thanks also to Paul Kuin for use of his software and significant help and discussion about *Swift*/UVOT grism analysis. We thank Mike Goad and Kirk Korista for insightful discussions on the lack of Mg II variability and also thank the referee for suggesting Fe II template fitting. EMC gratefully acknowledges support provided by NASA through grant NNX14AC23G to Wayne State University. MCB gratefully acknowledges support from the NSF through CAREER grant AST-1253702 to Georgia State University. BMP gratefully acknowledges support from the NSF through grant AST-1008882 to The Ohio

State University. MV gratefully acknowledges support from the Danish Council for Independent Research via grant no. DFF 4002-00275.

REFERENCES

- Assef, R. J. et al. 2011, *ApJ*, 742, 93
 Baldassare, V., Reines, A., Gallo, E., & Greene, J. 2015, *ApJ Letter*, in press, arXiv:1506.07531
 Baldwin, J. A., Ferland, G. J., Korista, K. T., Hamann, F., & LaCluzé, A. 2004, *ApJ*, 615, 610
 Barth, A. J. et al. 2011, *ApJ*, 732, 121
 —. 2013, *ApJ*, 769, 128
 —. 2015, *ApJS*, 217, 26
 Bentz, M. C., Denney, K. D., Cackett, E. M., et al. 2006a, *ApJ*, 651, 775
 Bentz, M. C. & Katz, S. 2015, *PASP*, 127, 67
 Bentz, M. C., Peterson, B. M., Netzer, H., Pogge, R. W., & Vestergaard, M. 2009a, *ApJ*, 697, 160
 Bentz, M. C., Peterson, B. M., Pogge, R. W., Vestergaard, M., & Onken, C. A. 2006b, *ApJ*, 644, 133
 Bentz, M. C. et al. 2007, *ApJ*, 662, 205
 —. 2009b, *ApJ*, 705, 199
 —. 2010, *ApJ*, 716, 993
 —. 2013, *ApJ*, 767, 149
 Blandford, R. D. & McKee, C. F. 1982, *ApJ*, 255, 419
 Brewer, B. J., Treu, T., Pancoast, A., Barth, A. J., Bennert, V. N., Bentz, M. C., Filippenko, A. V., Greene, J. E., Malkan, M. A., & Woo, J.-H. 2011, *ApJ*, 733, L33
 Cackett, E. M., Horne, K., & Winkler, H. 2007, *MNRAS*, 380, 669
 Clavel, J. et al. 1991, *ApJ*, 366, 64
 De Rosa, G. et al. 2015, *ApJ*, 806, 128
 Denney, K. D. 2012, *ApJ*, 759, 44
 Denney, K. D., Pogge, R. W., Assef, R. J., Kochanek, C. S., Peterson, B. M., & Vestergaard, M. 2013, *ApJ*, 775, 60
 Edelson, R. et al. 2015, *ApJ*, 806, 129
 Gebhardt, K., Bender, R., Bower, G., Dressler, A., Faber, S. M., Filippenko, A. V., Green, R., Grillmair, C., Ho, L. C., Kormendy, J., Lauer, T. R., Magorrian, J., Pinkney, J., Richstone, D., & Tremaine, S. 2000, *ApJ*, 539, L13
 Goad, M. R., Koratkar, A. P., Axon, D. J., Korista, K. T., & O'Brien, P. T. 1999a, *ApJ*, 512, L95
 Goad, M. R., Koratkar, A. P., Kim-Quijano, J., Korista, K. T., O'Brien, P. T., & Axon, D. J. 1999b, *ApJ*, 524, 707
 Goad, M. R., O'Brien, P. T., & Gondhalekar, P. M. 1993, *MNRAS*, 263, 149
 Greene, J. E. & Ho, L. C. 2007, *ApJ*, 670, 92
 Greene, J. E., Peng, C. Y., & Ludwig, R. R. 2010, *ApJ*, 709, 937
 Grier, C. J., Martini, P., Watson, L. C., Peterson, B. M., Bentz, M. C., Dasyra, K. M., Dietrich, M., Ferrarese, L., Pogge, R. W., & Zu, Y. 2013, *ApJ*, 773, 90
 Guerras, E., Mediavilla, E., Jimenez-Vicente, J., Kochanek, C. S., Muñoz, J. A., Falco, E., & Motta, V. 2013, *ApJ*, 764, 160
 Gültekin, K., Gebhardt, K., Kormendy, J., Lauer, T. R., Bender, R., Tremaine, S., & Richstone, D. O. 2014, *ApJ*, 781, 112
 Gültekin, K. et al. 2009, *ApJ*, 698, 198
 Hryniewicz, K., Czerny, B., Pych, W., Udalski, A., Krupa, M., Świątoń, A., & Kaluzny, J. 2014, *A&A*, 562, A34
 Kaastra, J. S. et al. 2014, *Science*, 345, 64
 Kaspi, S., Brandt, W. N., Maoz, D., Netzer, H., Schneider, D. P., & Shemmer, O. 2007, *ApJ*, 659, 997
 Kaspi, S., Smith, P. S., Netzer, H., Maoz, D., Jannuzi, B. T., & Giveon, U. 2000, *ApJ*, 533, 631
 Kokubo, M., Morokuma, T., Minezaki, T., Doi, M., Kawaguchi, T., Sameshima, H., & Koshida, S. 2014, *ApJ*, 783, 46
 Kollatschny, W. 2003, *A&A*, 407, 461
 Korista, K. T. & Goad, M. R. 2000, *ApJ*, 536, 284
 Kormendy, J. & Ho, L. C. 2013, *ARA&A*, 51, 511
 Kuin, N. P. M. 2014, *Astrophysics Source Code Library*, record ascl:1410.004
 Kuin, N. P. M. et al. 2015, *MNRAS*, submitted, arXiv:1501.02433
 Magorrian, J., Tremaine, S., Richstone, D., Bender, R., Bower, G., Dressler, A., Faber, S. M., Gebhardt, K., Green, R., Grillmair, C., Kormendy, J., & Lauer, T. 1998, *AJ*, 115, 2285
 Marziani, P., Sulentic, J. W., Plauchu-Frayn, I., & del Olmo, A. 2013, *A&A*, 555, A89
 McGill, K. L., Woo, J.-H., Treu, T., & Malkan, M. A. 2008, *ApJ*, 673, 703
 McHardy, I. M., Cameron, D. T., Dwelly, T., Connolly, S., Lira, P., Emmanoulopoulos, D., Gelbord, J., Breedt, E., Arevalo, P., & Uttley, P. 2014, *MNRAS*, 444, 1469
 McLure, R. J. & Jarvis, M. J. 2002, *MNRAS*, 337, 109
 Mehdipour, M. et al. 2015, *A&A*, 575, A22
 Metzroth, K. G., Onken, C. A., & Peterson, B. M. 2006, *ApJ*, 647, 901
 Modzelewska, J., Czerny, B., Hryniewicz, K., Bilicki, M., Krupa, M., Świątoń, A., Pych, W., Udalski, A., Adhikari, T. P., & Petrogalli, F. 2014, *A&A*, 570, A53
 O'Brien, P. T., Goad, M. R., & Gondhalekar, P. M. 1995, *MNRAS*, 275, 1125
 Onken, C. A. & Kollmeier, J. A. 2008, *ApJ*, 689, L13
 Pancoast, A., Brewer, B. J., Treu, T., Park, D., Barth, A. J., Bentz, M. C., & Woo, J.-H. 2014, *MNRAS*, 445, 3073
 Park, D., Woo, J.-H., Denney, K. D., & Shin, J. 2013, *ApJ*, 770, 87
 Peterson, B. M. 1993, *PASP*, 105, 247
 —. 2014, *Space Sci. Rev.*, 183, 253
 Peterson, B. M. & Wandel, A. 1999, *ApJ*, 521, L95
 —. 2000, *ApJ*, 540, L13
 Peterson, B. M. et al. 2002, *ApJ*, 581, 197
 —. 2004, *ApJ*, 613, 682
 Rafiee, A. & Hall, P. B. 2011, *ApJS*, 194, 42
 Reichert, G. A. et al. 1994, *ApJ*, 425, 582
 Schlegel, D. J., Finkbeiner, D. P., & Davis, M. 1998, *ApJ*, 500, 525
 Seaton, M. J. 1979, *MNRAS*, 187, 73P
 Shen, Y. & Liu, X. 2012, *ApJ*, 753, 125
 Trakhtenbrot, B. & Netzer, H. 2012, *MNRAS*, 427, 3081
 Trevese, D., Paris, D., Stirpe, G. M., Vagnetti, F., & Zitelli, V. 2007, *A&A*, 470, 491
 Vaughan, S., Edelson, R., Warwick, R. S., & Uttley, P. 2003, *MNRAS*, 345, 1271
 Vestergaard, M. 2002, *ApJ*, 571, 733
 Vestergaard, M. & Osmer, P. S. 2009, *ApJ*, 699, 800
 Vestergaard, M. & Peterson, B. M. 2005, *ApJ*, 625, 688
 —. 2006, *ApJ*, 641, 689
 Vestergaard, M. & Wilkes, B. J. 2001, *ApJS*, 134, 1
 Walsh, J. L., Barth, A. J., Ho, L. C., & Sarzi, M. 2013, *ApJ*, 770, 86
 Wang, J.-G., Dong, X.-B., Wang, T.-G., Ho, L. C., Yuan, W., Wang, H., Zhang, K., Zhang, S., & Zhou, H. 2009, *ApJ*, 707, 1334
 Welsh, W. F. 1999, *PASP*, 111, 1347
 White, R. J. & Peterson, B. M. 1994, *PASP*, 106, 879
 Woo, J.-H. 2008, *AJ*, 135, 1849
 Woo, J.-H., Yoon, Y., Park, S., Park, D., & Kim, S. C. 2015, *ApJ*, 801, 38